Imprinting a topological interface using Zeeman shifts in an atomic spinor Bose–Einstein condensate

M O Borgh, J Lovegrove and J Ruostekoski

Mathematical Sciences, University of Southampton, Southampton SO17 1BJ, UK

Abstract

We propose to use spatial control of the Zeeman energy shifts in an ultracold atomic gas to engineer an interface between topologically distinct regions. This provides an experimentally accessible means for studying the interface physics of topological defects and textures. Using the spin-1 Bose–Einstein condensate as an example, we find spinor wave functions that represent defects and textures continuously connecting across the interface between polar and ferromagnetic regions induced by spatially varying Zeeman shifts. By numerical energy-minimization we characterize the defect core structures and determine the energetic stability. The techniques proposed could potentially be used in the laboratory to emulate complex interface physics arising, e.g., in cosmological and condensed-matter contexts in both uniform and lattice systems.

Keywords: atomic spinor Bose–Einstein condensates, topological defects and textures, topological interface

1. Introduction

The physics of topological defects, such as vortices, becomes especially intriguing at the interface between coexisting, topologically distinct phases of a macroscopically coherent system. Due to different broken symmetries on either side, a defect cannot perforate the interface unchanged. Instead it must either terminate, or continuously connect across the

boundary to an object representing a different topology. This situation arises, for example, at the interface between the *A* and *B* phases of superfluid liquid ^{3}He [1–3], at interfaces between regions of different vacua in theories of the early universe [4, 5], in the physics of branes in superstring theory [6, 7], and in exotic superconductivity [8].

The parallels [2] between cosmological objects and defects in superfluids prompted the suggestion that analogues of cosmological phenomena can be studied in the laboratory [2, 9], for example the formation of defects in phase transitions [10–13] or properties of cosmic vortons (superconducting cosmic strings [14]) [15–19]. Current experimental techniques in atomic physics allow accurate measurements and precise control and manipulation of ultracold atomic gases by finely tuning electromagnetic fields. In spinor Bose–Einstein condensates (BECs), where the atoms retain their spin degree of freedom, experiments have demonstrated controlled preparation of coreless vortices and analogous non-singular textures formed by the nematic axis [20–23]. Vortex nucleation in phase transitions [13] and dynamical formation of spin textures [24–27] have also been experimentally observed. Simultaneously there has been a rapidly increasing theoretical interest in the wide variety of vortices, point defects and particle-like textures in two-component (pseudospin-1/2) [15–19, 28–31], as well as spin-1 [32–51] and spin-2,3 [52–56] BECs. This development brings multi-component systems of ultracold atoms to the forefront as candidate laboratories where properties of a variety of field-theoretical solitons (see for example [14, 57–60]) may be studied.

We have previously suggested [61, 62] that spatially non-uniform manipulation of scattering lengths by optical or microwave-induced Feshbach resonances can be used to study the physics of topological interfaces in ultracold atomic gases with spin degree of freedom. An example is the spinor BECs, which exhibit distinct phases of the ground-state manifold. In the simplest case of a spin-1 BEC there are two phases, polar and FM, and the sign of the spin-dependent interaction determines which phase is energetically favourable. We proposed that a combination of (microwave or optical) Feshbach resonances and spatially-dependent AC-Stark shifts can be used to enforce different signs of this interaction in different spatial regions of the same spin-1 BEC, establishing a coherent interface between the phases. Within this system, we formulated spinor wave functions corresponding to defect combinations that can be phase imprinted using existing techniques. By numerical simulation we found examples of energetically stable interface-crossing defects and complex core deformations, such as the formation of an arch-shaped half-quantum vortex on the interface. In addition, defects at an energetically established boundary in a two-component BEC, where in one region the two components are miscible and in the other immiscible, have recently been studied in BECs in [63–67].

Here we propose to employ precise spatial engineering of the Zeeman shifts to create topologically dissimilar regions within a spinor BEC, providing an experimentally simple route for studying defects and textures at the emerging topological interface. The ground state of the spinor BEC generally depends on the linear and quadratic energy shifts of the Zeeman levels. In the case of the spin-1 BEC, the Zeeman shift can cause the condensate to adopt the FM phase even when the polar phase is favoured by the interactions, and vice versa [13, 68–72].

In particular, we demonstrate that a stable, coherent, topologically non-trivial interface between FM and polar phases of a spin-1 BEC can be established through spatially non-uniform linear or quadratic Zeeman shifts. Uniform ground-state solutions exist, for both polar and FM interaction regimes, that follow the variation of the Zeeman shift; the corresponding wave

functions continuously interpolate between the polar and FM phases. We then analytically construct defect states that continuously connect defects and textures representing the topology of the FM and polar phases, such that the connection is provided directly by the spatial dependence of the Zeeman energy shifts. We show that the modulation of the Zeeman splitting allows the preparation of a rich family of interface-crossing defect solutions, with various combinations of singular (integer and half-quantum) and non-singular vortices, point defects, and terminating vortices. By numerical simulation, we determine the stability properties of the constructed solutions and determine their energy-minimizing core structures.

In the polar interaction regime, the interface is established by a varying linear Zeeman shift. Examples of energetically stable interface-perforating defect configurations in a rotating trap include a singly quantized FM vortex line continuously connecting to a singly quantized polar vortex whose core splits into a pair of half-quantum vortices, as well as a polar vortex that terminates at the interface.

For a BEC in the FM interaction regime, a spatially varying quadratic energy shift is used to establish the interface between the polar and FM phases. We find an energetically stable, singular FM vortex that terminates at the interface. Moreover, non-singular, coreless vortices in the FM phase become energetically favourable, and we find energetically stable structures where the coreless vortex continuously connects to a singly quantized vortex on the polar side of the interface. The unusual property of the singly quantized polar vortex in this configuration is the axially symmetric stable vortex core, in which the line singularity is filled with atoms in the FM phase, and the core is not split into a pair of half-quantum vortices.

The existence of stable core structures of different symmetries in atomic spinor BECs is reminiscent of the rich vortex core symmetries encountered in superfluid liquid ^{3}He [73]. For example, the core of a singular *B*-phase vortex may analogously retain a non-zero superfluid density by filling with the *A* phase, either with an axially symmetric core [74] or by breaking the axial symmetry when forming a two-fold symmetric split core [75, 76].

In the case of both FM and polar interactions we also find stable core structures of singular FM vortex lines terminating on a point defect in the polar phase. Such a point defect is analogous to the 't Hooft–Polyakov monopole [77, 78] and the combined defect configuration of the terminating vortex line and the point defect is closely related to boojums that can exist in superfluid liquid ^{3}He [2, 79, 80]. The core of the point defect minimizes its energy by deforming into a half-quantum line defect connecting at both ends to the interface. As the point defect, or the 'Alice arch' line defect, does not couple to the trap rotation, the defect experiences a trivial instability with respect to drifting out of the atom cloud as a result of the density gradient of the harmonic trap (the order parameter bending energy of defects and textures generally favours lower atom densities), but can be otherwise stable. Such an instability could be overcome by creating a local density minimum close to the trap centre by an additional optical potential [40].

The interface physics with the Zeeman shifts provides several promising experimental scenarios. Accurate tuning of Zeeman shifts has been experimentally demonstrated in ultracold atoms [81], and also applied to the study of spin textures [27]. On the other hand, the control of multiple interfaces and their time-dependence could open up avenues for emulating complex cosmological phenomena in the laboratory. For instance, in superfluid liquid ^{3}He [82] or in a two-component BEC system [63–66] it has been proposed that colliding interfaces or phase

boundaries could mimic cosmic defect formation. In a spin-1 BEC we could envisage, for instance, the following set-up: a disc of polar phase is created in an otherwise FM condensate by locally increasing Zeeman shift. The two parallel FM-polar interfaces can then be interpreted as analogues of string-theoretical *D*-branes and anti-branes arising in theories of brane inflation [6]. Removing the local Zeeman shift causes the interfaces to collapse, simulating defect formation in brane annihilation scenarios. Similar experiments have been performed with colliding superfluid ^{3}He *A–B* interfaces [82], where, however, observation of defects is more difficult.

2. Effects of Zeeman energy shifts in the spin-1 BEC

Here we consider the engineering of a topological interface by manipulation of Zeeman shifts in the context of a spin-1 BEC. In the Gross–Pitaevskii mean-field theory, the condensate wave function is a three-component vector $\Psi = \sqrt{n}\,\zeta$, where n is the atomic density and ζ is a normalized spinor ($\zeta^\dagger \zeta = 1$) in the basis of spin projection onto the z axis. A magnetic field in the z direction leads to linear and quadratic energy shifts of the Zeeman sublevels, of strengths p and q respectively. The Hamiltonian density may then be written as [83]

$$\mathcal{H} = \frac{\hbar^2}{2m}\left|\nabla\Psi\right|^2 + V(\mathbf{r})n + \frac{c_0}{2}n^2 + \frac{c_2}{2}n^2\left|\left\langle\hat{\mathbf{F}}\right\rangle\right|^2 - pn\left\langle\hat{F}_z\right\rangle + qn\left\langle\hat{F}_z^2\right\rangle, \quad (1)$$

where $V(\mathbf{r})$ is the external trapping potential for the atoms. The local spin vector is given by the expectation value of the spin operator $\hat{\mathbf{F}}$ defined as a vector of spin-1 Pauli matrices. The contact interaction between the atoms separates into spin-independent and spin-dependent contributions. The respective interaction strengths are $c_0 = 4\pi\hbar^2\left(2a_2 + a_0\right)/3m$ and $c_2 = 4\pi\hbar^2\left(a_2 - a_0\right)/3m$, where m is the atomic mass, and $a_{0,2}$ are the scattering lengths in the spin-0, 2 channels of colliding spin-1 atoms. The interaction terms give rise to the density and spin healing lengths

$$\xi_n = \frac{\hbar}{\sqrt{2mc_0 n}}, \qquad \xi_F = \frac{\hbar}{\sqrt{2\,m|c_2|n}}, \quad (2)$$

that describe the length scales over which perturbations of the atom density and the spin magnitudes, respectively, heal.

When the Zeeman shifts are not present ($p = q = 0$), (1) is invariant under spin rotations. The ground state of the uniform system ($V(\mathbf{r}) = 0$) then exhibits two phases depending on the sign of c_2. In the FM phase, favoured when $c_2 < 0$ (e.g., in ^{87}Rb), the spin is maximized: $\left|\left\langle\hat{\mathbf{F}}\right\rangle\right| = 1$ for a uniform spin texture. All physically distinguishable, degenerate, ground states are then coupled by three-dimensional spin rotations. The family of FM spinors can therefore be parametrized as [32]

$$\zeta^{\mathrm{f}} = \frac{e^{i\phi'}}{\sqrt{2}} \begin{pmatrix} \sqrt{2}\, e^{-i\alpha} \cos^2\frac{\beta}{2} \\ \sin\beta \\ \sqrt{2}\, e^{i\alpha} \sin^2\frac{\beta}{2} \end{pmatrix}, \tag{3}$$

where $\left(\alpha, \beta, \phi'\right)$ are Euler angles defining the spin rotation such that $\left\langle \hat{\mathbf{F}} \right\rangle = \cos\alpha \sin\beta\, \hat{\mathbf{x}} + \sin\alpha \sin\beta\, \hat{\mathbf{y}} + \cos\beta\, \hat{\mathbf{z}}$. A condensate phase ϕ is absorbed by the third Euler angle γ to form $\phi' = \phi - \gamma$, and corresponds to spin rotations about the local spin direction. The order-parameter manifold, the broken symmetry in the ground state, is therefore $\mathrm{SO}(3)$, which supports only two distinct classes of line defects: singular, singly quantized vortices, and non-singular coreless vortices (see appendix A).

The polar phase with minimized spin, $\left| \left\langle \hat{\mathbf{F}} \right\rangle \right| = 0$ in the uniform texture, is favoured when $c_2 > 0$ (e.g., in ^{23}Na). The degenerate ground states are then characterized by a macroscopic condensate phase ϕ and a unit vector $\hat{\mathbf{d}}$ [35, 40]:

$$\zeta^{\mathrm{p}} = \frac{e^{i\phi}}{\sqrt{2}} \begin{pmatrix} -d_x + id_y \\ \sqrt{2}\, d_z \\ d_x + id_y \end{pmatrix}. \tag{4}$$

Note that $\zeta\left(\phi, \hat{\mathbf{d}}\right) = \zeta\left(\phi + \pi, -\hat{\mathbf{d}}\right)$. These states are therefore identified, and hence $\hat{\mathbf{d}}$ should be understood as unoriented. The identification is reflected in the factorization by the two-element group in the corresponding broken ground-state symmetry $\left[S^2 \times \mathrm{U}(1) \right]/\mathbb{Z}_2$. This so-called nematic order leads to the existence of half-quantum vortices [e.g., (A.6)]. While all circulation-carrying vortices are singular in the polar phase, it is possible to form a non-singular *nematic coreless vortex* [51], characterized by a fountain-like texture in $\hat{\mathbf{d}}$ (e.g. (A.7)).

Here we consider the case when either or both of the Zeeman energy contributions are non-zero. The linear Zeeman shift in a magnetic field $\mathbf{B} = B\hat{\mathbf{z}}$ is given by $p = -g_F \mu_B B$, where the Landé factor $g_F = -1/2$ in the $F = 1$ ground-state manifold of ^{23}Na or ^{87}Rb. The linear shift can be given a spatial dependence by careful engineering of the applied magnetic field $\mathbf{B}$. In alkali-metal atoms in the regime relevant to our considerations, the quadratic shift q, which can be obtained from the Breit–Rabi formula [84], is positive and smaller than p. However, by combining a static magnetic field with an off-resonant microwave dressing field, accurate tuning of the quadratic energy shift can be achieved through the resulting AC-Stark shifts [81], or could be induced by lasers [85].

When the Zeeman shifts are included, the coupled Gross–Pitaevskii equations for the spinor components $\psi_j = n\zeta_i$ ($j = +, 0, -$) derived from (1) read

$$i\hbar \frac{\partial}{\partial t} \Psi = \left[-\frac{\hbar^2}{2m} \nabla^2 + V(\mathbf{r}) + c_0 n + c_2 n \left\langle \hat{\mathbf{F}} \right\rangle \cdot \hat{\mathbf{F}} - p\hat{F}_z + q\hat{F}_z^2 \right] \Psi. \tag{5}$$

In a uniform system, these may be solved analytically [70–72] to find the stationary states. The Zeeman shifts break the spin-rotational symmetry of the FM and polar ground states. One then finds, in addition to the purely FM state with $\left\langle \hat{\mathbf{F}} \right\rangle = \pm\hat{\mathbf{z}}$ and the polar state with $\hat{\mathbf{d}} = \hat{\mathbf{z}}$, also the

steady-state solution [70, 72]

$$\zeta = \frac{1}{\sqrt{2}} \begin{pmatrix} e^{i\chi_+} P_+ \\ 0 \\ e^{i\chi_-} P_- \end{pmatrix}, \tag{6}$$

where $P_\pm = \sqrt{1 \pm p/c_2 n}$. The solution (6) is valid provided that the linear Zeeman shift is sufficiently small, such that $|p| \leqslant c_2 n$. Note that the expectation value of the spin is no longer zero, $\langle \hat{\mathbf{F}} \rangle = p/(c_2 n)\hat{\mathbf{z}}$, and $\hat{\mathbf{d}}$ lies in the xy plane. For very weak linear Zeeman shift p, the expression then approaches the polar state $\zeta = \left(e^{i\chi_+}/\sqrt{2}, 0, e^{i\chi_-}/\sqrt{2} \right)^T$. At the limit of validity, on the other hand, it coincides with the FM solution $\zeta = \left(e^{i\chi_+}, 0, 0 \right)^T$ for $p > 0$ [$\zeta = \left(0, 0, e^{i\chi_-} \right)^T$ for $p < 0$]. The spinor (6) also represents the lowest-energy state when $c_2 > 0$ and $q \leqslant p^2/2c_2 n$ [70, 72]. Hence in a condensate with polar interactions, such as for ^{23}Na, (6) provides an energetically stable solution that takes values between FM and polar phases, depending on the linear Zeeman shift.

A further solution with variable $\left| \langle \hat{\mathbf{F}} \rangle \right|$ is given by the FM-like spinor [71, 72]

$$\begin{aligned} \zeta_\pm &= e^{i(\chi_0 \mp \chi_z)} (q \pm p) \sqrt{\frac{-p^2 + q^2 + 2c_2 nq}{8c_2 nq^3}}, \\ \zeta_0 &= e^{i\chi_0} \sqrt{\frac{(q^2 - p^2)(-p^2 - q^2 + 2c_2 nq)}{4c_2 nq^3}}. \end{aligned} \tag{7}$$

The solution is valid when the expressions under the square roots are positive. The corresponding regions in the (p, q) plane are shown in figure 1. While several regions of validity exist for both signs of c_2, we note that (7) forms the ground state in the uniform system only for $c_2 < 0$ in the region defined by $|q| > |p|$ and $p^2 > q^2 - 2|c_2|nq$. From this point on, we will consider the solution (7) only in this parameter range. The spin vector is in general tilted with respect to the magnetic field and for $\chi_0 = \chi_z = 0$ lies in the xz plane for the parameters of interest. Then

$$\langle \hat{\mathbf{F}} \rangle = \frac{\sqrt{(q^2 - p^2)\left[(p^2 - 2c_2 nq)^2 - q^4 \right]}}{2|c_2|nq^2} \hat{\mathbf{x}} + \frac{p(-p^2 + q^2 + 2qc_2 n)}{2c_2 nq^2} \hat{\mathbf{z}}, \tag{8}$$

such that

$$\left| \langle \hat{\mathbf{F}} \rangle \right| = \sqrt{\frac{2q^2(p^2 + 2c_2^2 n^2) - q^4 - p^4}{4q^2 c_2^2 n^2}}. \tag{9}$$

Assuming $p > 0$ ($p < 0$ analogous by symmetry), the limit ($p = q$) yields $\left| \langle \hat{\mathbf{F}} \rangle \right| = 1$, corresponding to the FM state $\zeta = (1, 0, 0)^T$. Similarly, $p^2 = q^2 - 2|c_2|nq$ yields the polar
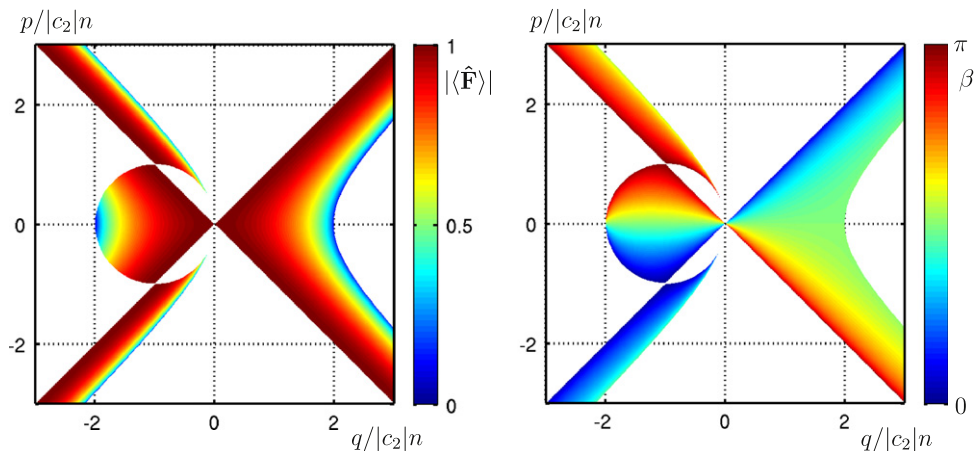
Figure 1. The solution (7) is valid in the coloured regions. Left: spin magnitude showing interpolation between FM and polar limits. Right: angle β between $\langle \hat{\mathbf{F}} \rangle$ and $\hat{\mathbf{z}}$. The figure shows the case $c_2 < 0$ where (7) forms the ground state for $q > 0$. For $c_2 > 0$, the figures are mirrored around the origin, and the solution is never the ground state.

limit $\zeta = (0, 1, 0)^T$ with $\left| \langle \hat{\mathbf{F}} \rangle \right| = 0$ and $\hat{\mathbf{d}} = \hat{\mathbf{z}}$. From these results it follows (see also figure 1) that varying p and/or q can continuously connect the two limits while simultaneously rotating the spin vector from $\langle \hat{\mathbf{F}} \rangle = \hat{\mathbf{z}}$ in the FM limit to the x direction (implying a simultaneous rotation of $\hat{\mathbf{d}}$ from $-\hat{\mathbf{x}}$ to $\hat{\mathbf{z}}$). For simplicity, we will here only consider variations of q for constant p.

Together (6) and (7) thus provide us with spinor wave functions that—in the polar and FM interaction regimes, respectively—represent solutions of different spin magnitudes $\left| \langle \hat{\mathbf{F}} \rangle \right|$, depending on the value of the Zeeman shifts. Here we propose to create the topological interface between FM and polar phases by engineering the spatial dependence of the linear and quadratic level shifts. For spatially varying Zeeman energy shifts the solutions (6) and (7) continuously interpolate between the polar and FM phases. We will show that a stable, coherent interface forms in the intermediate region. It then becomes possible for topological defects and textures in the two regions of the polar and FM phases to connect continuously across the interface. We now proceed to explicitly construct such analytic defect solutions for the two interaction regimes separately.

3. Interface by linear Zeeman shift for $c_2 > 0$

In order to construct defect states in the BEC with polar interactions it is beneficial to transform the ground-state solution (6) by applying a BEC phase ϕ and a rotation [determined by the Euler angles (α, β, γ)] of the orthogonal vector triad $\left(\langle \hat{\mathbf{F}} \rangle, \hat{\mathbf{d}}, \langle \hat{\mathbf{F}} \rangle \times \hat{\mathbf{d}} \right)$. We obtain

Table 1. Interface-crossing defects in the polar interaction regime ($c_2 > 0$) are constructed from (10) by different choices for ϕ, α, and γ (given as multiples of the azimuthal angle φ). For states with non-constant β, its functional form is given in the table, where $\beta(\rho)$ denotes a monotonically increasing function of the radial distance only (see text for details). The two solutions with a Dirac monopole in the FM limit differ by aligning the doubly quantized Dirac string with the positive and negative z axis, respectively (cf (A.3)).

FM limit	Polar limit	ϕ/φ	α/φ	γ/φ	β
Vortex free	Half-quantum vortex	1/2	0	1/2	const.
Vortex free	Singly quantized vortex	1	0	1	const.
Coreless vortex	Half-quantum vortex	1/2	1	−1/2	$\beta(\rho)$
Coreless vortex	Singly quantized vortex	1	1	0	$\beta(\rho)$
Coreless vortex	Nematic coreless vortex	0	1	−1	$\beta(\rho)$
Singular vortex	Nematic coreless vortex	0	1	0	$\beta(\rho)$
Singular vortex	Half-quantum vortex	1/2	1	1/2	const.
Singular vortex	Half-quantum vortex	1/2	0	−1/2	const.
Singular vortex	Singly quantized vortex	1	0	0	const.
Singular vortex	Point defect	0	1	0	$\beta = \theta - \frac{\pi}{2}$
Dirac monopole (z_+)	Singly quantized vortex	−1	1	0	$\beta = \theta$
Dirac monopole (z_-)	Singly quantized vortex	−1	−1	0	$\beta = \theta$

$$
\zeta = \frac{e^{i\phi}}{2}
\begin{pmatrix}
\sqrt{2}\, e^{-i\alpha} \left(e^{i\gamma} \sin^2\frac{\beta}{2} P_- - e^{-i\gamma} \cos^2\frac{\beta}{2} P_+ \right) \\
-\sin\beta \left(e^{i\gamma} P_- + e^{-i\gamma} P_+ \right) \\
\sqrt{2}\, e^{i\alpha} \left(e^{i\gamma} \cos^2\frac{\beta}{2} P_- - e^{-i\gamma} \sin^2\frac{\beta}{2} P_+ \right)
\end{pmatrix},
\tag{10}
$$

where we have set $\chi_+ = \pi$, $\chi_- = 0$ to specify $\hat{\mathbf{d}} = \hat{\mathbf{x}}$ in (6). For (10) we have

$$
\left\langle \hat{\mathbf{F}} \right\rangle = F \cos\alpha \sin\beta \hat{\mathbf{x}} + F \sin\alpha \sin\beta \hat{\mathbf{y}} + F \cos\beta \hat{\mathbf{z}},
\tag{11}
$$

$$
\begin{aligned}
\hat{\mathbf{d}} =\ & (\cos\alpha \cos\beta \cos\gamma - \sin\alpha \sin\gamma)\hat{\mathbf{x}} \\
& + (\sin\alpha \cos\beta \cos\gamma + \cos\alpha \sin\gamma)\hat{\mathbf{y}} - \sin\beta \cos\gamma \hat{\mathbf{z}}.
\end{aligned}
\tag{12}
$$

Equation (10) represents a spinor wave function that takes values between the FM and the polar phases while allowing the spatial variation of the orientation of the triad and the BEC phase, as determined by $(\phi, \alpha, \beta, \gamma)$. In the absence of the Zeeman shifts, it gives all the degenerate states. The Zeeman energy contribution can partially lift this degeneracy, but as we will consider non-uniform defect states in a rotating trap, (10) provides the most suitable starting point for constructing the initial states for the energy minimization.

We can now construct specific defect configurations, that connect FM and polar defects by making appropriate choices for $(\phi, \alpha, \beta, \gamma)$. All the basic defect connections that we have engineered are presented in table 1. The elementary defect and textures of the spin-1 system that act as building blocks are briefly summarized in appendix A. Here we give an explicit discussion of some representative examples. The procedure for constructing the vortex

connections is to first identify the essential characteristics of the limiting defect states and then the necessary parameter choices in (10).

Singly quantized vortex penetrating the interface: the phase vortex, formed by a 2π winding of the condensate phase alone, corresponds to a singular, singly quantized vortex in both FM and polar limits (see appendix A). Hence, we may continuously connect the two across the interface formed as p is varied by choosing $\phi = \varphi$, where φ is the azimuthal angle in polar coordinates, and keeping the Euler angles α, β and γ constant in (10). Making the simplifying assumption $\alpha = \gamma = 0$, we then have

$$
\zeta = \frac{e^{i\varphi}}{2}
\begin{pmatrix}
\sqrt{2}\left(\sin^2\frac{\beta}{2}P_- - \cos^2\frac{\beta}{2}P_+\right) \\
-\sin\beta\left(P_- + P_+\right) \\
\sqrt{2}\left(\cos^2\frac{\beta}{2}P_- - \sin^2\frac{\beta}{2}P_+\right)
\end{pmatrix}.
\tag{13}
$$

Note that this solution is deceptively simple: a singly quantized vortex represents entirely different objects (due to the different topology) in the two phases. More complicated vortex states can be constructed by more elaborate choices.

Singly quantized polar vortex to FM coreless vortex: the latter is characterized by a 2π winding of the condensate phase, together with a simultaneous spin rotation represented by a 2π winding of α, as described by (A.2). Hence we choose $\phi = \alpha = \varphi$ ($\gamma = 0$), giving

$$
\zeta = \frac{1}{2}
\begin{pmatrix}
\sqrt{2}\left(\sin^2\frac{\beta(\rho)}{2}P_- - \cos^2\frac{\beta(\rho)}{2}P_+\right) \\
-e^{i\varphi}\sin\beta(\rho)\left(P_- + P_+\right) \\
\sqrt{2}\,e^{i2\varphi}\left(\cos^2\frac{\beta(\rho)}{2}P_- - \sin^2\frac{\beta(\rho)}{2}P_+\right)
\end{pmatrix},
\tag{14}
$$

where we also require $\beta(\rho)$ to increase monotonically with the radial distance ρ, from $\beta = 0$ on the z axis, to form the characteristic fountain-like spin texture. In the polar limit, a 2π condensate-phase winding represents a singly quantized vortex. According to (A.5), the remaining 2π winding in α only associates a rotation of the $\hat{\mathbf{d}}$-vector with the singly quantized vortex. As p varies between $0 \leqslant |p| \leqslant c_2 n$, this singly quantized polar vortex connects across the interface to the coreless vortex in the FM limit.

Termination of a singular FM vortex as a point defect on the interface. A point defect in the polar phase corresponds to a radial hedgehog of the $\hat{\mathbf{d}}$ axis, analogous to the 't Hooft–Polyakov monopole [77, 78]. The simplest example is given in (A.8). In the polar limit of (10), we form the point defect by a 2π winding in α together with $\beta = \theta - \pi/2$, where θ is the polar angle in spherical coordinates. In the FM limit the same choices correspond to a singular spin texture similar to (A.1), exhibiting a radial disgyration around the singular line. We can thus construct a singular FM vortex that terminates as the upper half of a polar point defect by choosing $\alpha = \varphi$ and $\beta = \theta - \pi/2$.

Half-quantum vortex to singular FM vortex: the defining feature of a polar half-quantum vortex (A.6) is a π winding of the condensate phase ϕ, together with a simultaneous $\hat{\mathbf{d}} \to -\hat{\mathbf{d}}$ winding of the nematic axis to keep the order parameter single-valued. However, no similar construction is possible in the FM phase. Therefore the winding of the condensate phase must combine with the spin rotation represented by the third Euler angle γ to make the combined

$\phi' = \phi - \gamma$ in the FM limit (cf (3)) wind by a multiple of 2π. The combination $\phi = -\gamma = \varphi/2$ ($\alpha = 0$) connects the half-quantum vortex to a singly quantized vortex defined by $\phi' = \varphi$ in the FM limit.

Terminating half-quantum vortex: if we instead let $\gamma = \phi = \varphi/2$, so that these enter the spinor with the same sign, the polar limit of (10) remains a half-quantum vortex, with the rotation of $\hat{\mathbf{d}}$ being in the opposite sense. However, in the FM limit, ϕ and γ now cancel, $\phi' = 0$, and the order parameter represents a vortex-free state. The half-quantum vortex in the polar part thus terminates at the interface.

As shown in table 1, we also find solutions of a terminating singly quantized polar vortex, a half-quantum vortex connecting to a coreless vortex, a nematic coreless vortex (A.7) connecting either to a coreless or a singular vortex, and a Dirac monopole (A.3) continuously perforating the interface to a singly quantized polar vortex. Note that the vortex line (Dirac string) attached to the Dirac monopole may be formed in two ways: it can be included in the FM phase in such a way that the Dirac monopole joins the polar vortex to the FM vortex that forms the Dirac string. Alternatively, the polar vortex itself can act as a Dirac string, so that no other vortices need to be coupled to the monopole. In the latter case, the polar vortex terminates on the interface to a point defect.

4. Interface by quadratic Zeeman shifts for $c_2 < 0$

In the FM interaction regime ($c_2 < 0$), we proceed as in the polar case, but now transform the spinor wave function (7) by applying a BEC phase ϕ and rotations (α, β, γ) of the spinor to obtain

$$\zeta_{\pm} = \frac{e^{i\phi}}{2\sqrt{2}}\Big[e^{\mp i(\alpha+\gamma)}\big(\pm p + q\big)Q_+ \cos^2\frac{\beta}{2} + e^{\mp i(\alpha-\gamma)}\big(\mp p + q\big)Q_+ \sin^2\frac{\beta}{2}$$
$$\mp e^{\mp i\alpha}\sqrt{q^2 - p^2}\, Q_- \sin\beta \Big], \tag{15}$$

$$\zeta_0 = \frac{e^{i\phi}}{4}\Big\{ 2\sqrt{q^2 - p^2}\, Q_- \cos\beta + \big[e^{-i\gamma}(p + q) + e^{i\gamma}(p - q)\big]Q_+ \sin\beta \Big\}, \tag{16}$$

where

$$Q_{\pm} = \sqrt{\frac{-p^2 \pm q^2 + 2c_2 nq}{2c_2 nq^3}} . \tag{17}$$

Equation (8) gives the local spin direction $\mathbf{F}^0$ before the spin rotation, in terms of which the general spin texture can be expressed as

$$\big\langle \hat{\mathbf{F}} \big\rangle = \Big[\big(\cos\alpha \cos\gamma \cos\beta - \sin\alpha \sin\gamma\big)F_x^0 + \cos\alpha \sin\beta F_z^0 \Big]\hat{\mathbf{x}}$$
$$+ \Big[\big(\cos\alpha \sin\gamma \cos\beta + \sin\alpha \cos\gamma\big)F_x^0 + \sin\alpha \sin\beta F_z^0 \Big]\hat{\mathbf{y}}$$
$$+ \Big[-\cos\alpha \sin\beta F_x^0 + \cos\beta F_z^0 \Big]\hat{\mathbf{z}}. \tag{18}$$

A corresponding expression for $\hat{\mathbf{d}}$ may be derived by rotating the $\hat{\mathbf{d}}$-vector of (7). We can now make particular choices for α, β, γ and ϕ in order to construct specific defect states. The basic

Table 2. Interface-crossing defect configurations in the FM interaction regime ($c_2 < 0$) are constructed from (15) by different choices for ϕ, α, and γ (given as multiples of the azimuthal angle φ, except for $\gamma = \pi$). For states with non-constant β, its functional form is given in the table, where $\beta(\rho)$ denotes a monotonically increasing function of the radial distance only (see text for details). The two solutions with a Dirac monopole in the FM limit differ by aligning the doubly quantized Dirac string with the positive and negative z axis, respectively (cf (A.3)). Solutions involving half-quantum vortices are omitted since they cannot be straightforwardly constructed (see text).

FM limit	Polar limit	ϕ/φ	α/φ	γ/φ	β
Vortex free	Singly quantized vortex	1	0	1	const.
Coreless vortex	Singly quantized vortex	1	1	0	$\beta(\rho)$
Coreless vortex	Nematic coreless vortex	0	1	−1	$\beta(\rho)$
Singular vortex	Singly quantized vortex	1	0	0	const.
Singular vortex	Point defect	0	1	$\gamma = \pi$	$\beta = \theta$
Singular vortex	Nematic coreless vortex	0	1	0	$\beta(\rho)$
Dirac monopole (z_+)	Singly quantized vortex	−1	1	0	$\beta = \theta$
Dirac monopole (z_-)	Singly quantized vortex	−1	−1	0	$\beta = \theta$

interface-crossing defect configurations are presented in table 2. The derivation is very similar to the polar case and we only provide a brief example and highlight the differences in the case of half-quantum vortices.

FM coreless to singly quantized polar vortex: to form the coreless vortex (A.2) in the FM phase, we require $\alpha = \varphi$ together with a winding $\phi' = \phi - \gamma = \varphi$, as in the $c_2 > 0$ case. Note, however, that this equivalence between rotations of ϕ and γ holds only in the purely FM limit, and assigning the 2π winding to ϕ or γ leads to different vortex states in the polar limit (see table 2). In the former case, with $\gamma = 0$, we have

$$
\begin{aligned}
\zeta_+ &= \frac{1}{2\sqrt{2}}\left[(p+q)Q_+ \cos^2\frac{\beta(\rho)}{2} + (-p+q)Q_+ \sin^2\frac{\beta(\rho)}{2} \right. \\
&\quad \left. - \sqrt{q^2 - p^2}\, Q_- \sin\beta(\rho) \right], \\
\zeta_0 &= \frac{e^{i\phi}}{2}\left[\sqrt{q^2 - p^2}\, Q_- \cos\beta(\rho) + pQ_+ \sin\beta(\rho) \right], \\
\zeta_- &= \frac{e^{2i\varphi}}{2\sqrt{2}}\left[(-p+q)Q_+ \cos^2\frac{\beta(\rho)}{2} + (p+q)Q_+ \sin^2\frac{\beta(\rho)}{2} \right. \\
&\quad \left. + \sqrt{q^2 - p^2}\, Q_- \sin\beta(\rho) \right].
\end{aligned}
\tag{19}
$$

Similarly to (14), monotonically increasing $\beta(\rho)$ yields the required fountain-like texture in the FM limit. In the polar limit, the winding of the condensate phase implies that (19) reduces to (A.5), representing a singly quantized vortex, with which a 2π winding of $\hat{\mathbf{d}}$ is associated.

Half-quantum vortices: the polar half-quantum vortices may connect across the interface to coreless or singular vortices, or terminate at the interface, as in the polar interaction regime in

section 3. The analytic construction of these states from (15) in the FM interaction regime is less straightforward, as the dependence on γ in this case vanishes in the polar limit. The required π winding of $\hat{\mathbf{d}}$ must therefore instead be specified as $\beta = \varphi/2$, and β must then vary differently on the opposite sides of the interface, such that the wave function remains single-valued in the FM limit. These states will not be considered further here.

5. Preparation of vortex states

Several techniques have been proposed for controlled preparation of vortex states in BECs. These include transfer of angular momentum using Laguerre–Gaussian laser beams [86–88], combining mechanical rotation with coupling to an electromagnetic field [89], and rotation of the atomic spins by inverting a magnetic axial bias field [90]. Experimental implementations have demonstrated phase-imprinting of both singly and doubly quantized vortex lines [91–94], and in spinor BECs also preparation of non-singular textures [20–23]. These existing techniques could be used also to prepare defect states when an interface established by a non-uniform Zeeman shift is present. However, the relation between the analytically constructed defect solutions and the phase-imprinted states is different in the two interaction regimes ($c_2 \gtrless 0$).

In the polar interaction regime, the solutions of section 3 straightforwardly correspond to spin rotations of (6). Together with the condensate phase these result in singly or doubly quantized vortex lines in the individual spinor components, which may be directly phase imprinted using the existing techniques. For example, the interface-penetrating singly quantized vortex corresponds to a singly quantized vortex line in each of the spinor components. To connect a singly quantized polar vortex to a FM coreless vortex instead, vortex lines with phase winding of 2π and 4π respectively are imprinted in the $\zeta_{0,-}$ components (cf (14)).

The preparation of vortex states in the FM interaction regime is less straightforward. Due to the spin rotation implicit in the interpolating ground-state solution (7), the analytically constructed defect solutions cannot easily be phase imprinted directly. However, phase-imprintable defect wave functions representing the same defect states can be constructed by considering a target defect state in the FM or polar limit [61, 62].

Consider, e.g., the singly quantized FM vortex, constructed as a 2π winding of the condensate phase. For suitably chosen parameters, changing the sign of either of $\zeta_\pm$ causes the vortex wave function to switch from $\left| \left\langle \hat{\mathbf{F}} \right\rangle \right| = 1$ to $\left| \left\langle \hat{\mathbf{F}} \right\rangle \right| = 0$, such that it instead represents a singly quantized polar vortex. We can thus join the singly quantized vortices of the FM and polar phases by switching the sign of, e.g., ζ_- at the position of the interface to form

$$\zeta^{1 \leftrightarrow s} = \frac{e^{i\varphi}}{\sqrt{2}} \begin{pmatrix} \sqrt{2}\, e^{-i\alpha} \cos^2\frac{\beta}{2} \\ \sin \beta \\ \mp\sqrt{2}\, e^{i\alpha} \sin^2\frac{\beta}{2} \end{pmatrix}, \tag{20}$$

using the negative sign in the polar part of the condensate, and correspondingly the positive sign in the FM part. Note that the change of sign exactly yields a polar wave function only for $\beta = \pi/2$. However, also for any other $\sin(\beta) \neq 0$, the spinor wave function exhibits the spinor-component vortex lines required for the singly quantized vortex and quickly relaxes to the polar phase. Physically, the sign change in ζ_- corresponds to a dark soliton plane (a phase kink)

where the density in that particular spinor component vanishes. However, the density in the other two spinor components does not simultaneously vanish at the position of the soliton plane, and hence the full spinor wave function remains non-vanishing and continuous.

Approximate wave functions corresponding to other defect states may be constructed analogously. For example, when a singly quantized polar vortex is associated with a simultaneous rotation of the nematic axis, the spinor components exhibit the same vortex structure as the coreless FM vortex (A.2). Hence by again inserting a soliton plane in ζ_-, we obtain the interface spinor

$$\zeta^{1 \leftrightarrow \mathrm{cl}} = \frac{1}{\sqrt{2}} \begin{pmatrix} -\sin\beta \\ \sqrt{2}\, e^{i\varphi} \cos\beta \\ \pm\, e^{2i\varphi} \sin\beta \end{pmatrix}, \tag{21}$$

with the positive sign in the polar phase. With the negative sign, the wave function approximates the coreless vortex on the FM side, and quickly relaxes to $\left| \left\langle \hat{\mathbf{F}} \right\rangle \right| = 1$ and forms the characteristic fountain-like spin texture.

The construction is not limited to the connection of line defects across the interface. Also wave functions representing vortices terminating as point defects on the interface can be engineered. For example, the polar point defect (A.8) is formed by overlapping vortex lines of opposite winding in $\zeta_\pm$ together with a soliton plane in ζ_0. The point defect is placed on the interface by introducing a soliton plane also in ζ_+,

$$\zeta^{\mathrm{sv} \leftrightarrow \mathrm{pm}} = \frac{1}{\sqrt{2}} \begin{pmatrix} \mp e^{-i\varphi} \sin\theta \\ \sqrt{2}\, \cos\theta \\ e^{i\varphi} \sin\theta \end{pmatrix}, \tag{22}$$

such that the positive sign yields a wave function where the overlapping vortex lines approximate the singular vortex (A.1) on the FM side. On the polar side, the radial hedgehog $\hat{\mathbf{d}} = \hat{\mathbf{r}}$ in the nematic axis is retained.

These examples demonstrate that approximations to interface-crossing defect states may very generally be constructed from elementary building blocks of singly and doubly quantized vortex lines in the individual spinor components, together with a dark soliton plane (also phase-imprinted in experiments [95, 96]) at the position of the interface. Engineering vortex connections consisting of half-quantum vortices on the polar side is more involved. The preparation is complicated by the fact that there are no vortex solutions exhibiting π winding of the Euler angles that parametrize the FM order parameter. This implies that the construction will necessitate phase-imprinting of a vortex line that terminates at a soliton plane in one of the spinor components. Considering the connection of a half-quantum vortex (A.6) to a coreless vortex (A.2), we may then imagine proceeding as follows: by introducing a soliton plane in ζ_+ in (A.2), we again construct an interface spinor. However, on the polar side of the interface, we can now let a vortex line in ζ_+ terminate on the soliton plane. As a final step, we may use an optical shift to deplete the ζ_0 component in the polar part. The coreless vortex (A.2) then remains in the FM part of the cloud, while the spinor on the polar side of the interface approximates

$$\zeta = \frac{1}{\sqrt{2}} \begin{pmatrix} -e^{-i\varphi} \\ 0 \\ e^{2i\varphi} \end{pmatrix} = \frac{e^{i\varphi/2}}{\sqrt{2}} \begin{pmatrix} -e^{-3i\varphi/2} \\ 0 \\ e^{3i\varphi/2} \end{pmatrix}, \tag{23}$$

which represents a half-quantum vortex where $\hat{\mathbf{d}}$ exhibits a 3π winding into $-\hat{\mathbf{d}}$ as the vortex line is encircled. The continuity of the spinor wave function across the interface can be ensured by the ζ_- component, which exhibits only a doubly quantized vortex line and no soliton plane, and therefore does not vanish simultaneously across the entire interface.

6. Energetic stability and defect core structures

By the analytical constructions, we have demonstrated the existence of continuous wave functions representing topologically allowed interface-perforating defect connections (in tables 1 and 2). To determine their energetic stability, and the corresponding stable core structures, we minimize the energy of each defect state by integrating the coupled Gross–Pitaevskii equation (5) in imaginary time, in the frame rotating with frequency Ω. In experiment, the condensate is trapped by a harmonic potential, which we here take to be axially symmetric and slightly elongated along the z direction:

$$V(\mathbf{r}) = \frac{m\omega^2}{2}\left(x^2 + y^2 + \frac{1}{4}z^2\right). \tag{24}$$

We take the spin-independent nonlinearity to be $Nc_0 = 10^4 \hbar\omega l_\perp^3$, where $l_\perp = \sqrt{\hbar/m\omega}$ is the oscillator length in the transverse direction. We consider the experimentally relevant cases $c_0/c_2 = 28$, corresponding to ^{23}Na [97], and $c_0/c_2 = -216$, corresponding to ^{87}Rb [98], in the polar and FM regimes, respectively.

We can estimate the energy shifts required to establish the interface from (6) and (7). The gradients in p and q are then determined by the width of the interface region. In our numerics we have studied large widths of up to $10l_\perp$ and find that the qualitative features of the defect states remain unchanged. Since the width can be varied from large values down to the healing length scale, the possible values of the field gradient may cover a very large range of values. The experimentally most promising method to induce the energy shifts themselves is by using electromagnetic dressing fields, as demonstrated for the quadratic shift [81]. Potentially, similar methods could be used to manipulate also the linear shift, which may prove experimentally easier than using a static magnetic field.

For the case of FM interactions, we take the interface to be established by varying q at constant p (cf figure 1). We consider the example of ^{87}Rb and approximate the density profile by the Thomas–Fermi solution. Then for very small $p \sim 10^{-3}\hbar\omega$, the necessary difference in q is $\sim 0.15\hbar\omega$. For larger p the required change in q is smaller (while q itself is larger). For the recent experiment [27] the induced level shift is given in terms of the Rabi frequency Ω_R and detuning δ as $q = -\hbar\Omega_R^2/4\delta$, with $|\delta| = 2\pi \times 40$ kHz. As an example, we may consider a trap frequency $\omega = 2\pi \times 50$ Hz. We then find $\Omega_R^{polar} - \Omega_R^{FM} \simeq 6$ kHz.

In the case of polar interactions (6), $\left|\left\langle \hat{\mathbf{F}} \right\rangle\right|$ depends only on the linear Zeeman shift p, and reaches the FM phase for $p \gtrsim c_2 n$. Here we consider the example of ^{23}Na. Then the necessary

shift in p is $\sim 0.5\hbar\omega$ at the maximum value of the Thomas–Fermi density. Considering again the example $\omega = 2\pi \times 50$ Hz, this corresponds to a field gradient on the order of 1.4–14 G/m, for the corresponding variation 1–$10l_\perp$ of the interface width, if the shift is induced by a weak static magnetic field.

6.1. Polar interactions

When the spin-dependent interaction favours the polar phase, the interface is created by a spatially varying $0 \leqslant |p| \lesssim c_2 n$, corresponding to the ground-state solution (6). We then take the wave functions constructed in section 3 as initial states for the numerical energy minimization.

Even though singly quantized vortices exhibit similar winding of the condensate phase in both polar and FM phases, their energy-minimizing core structures are quite different [50]. In the polar BEC, the vortex may split to form an extended core region in which the wave function is excited out of the ground-state manifold. It reaches the FM phase on two singular half-quantum vortex lines. This lowers the energy by allowing the core size to be determined by the spin healing length ξ_F, defined in (2), which is usually larger than the size of a density-depleted core, given by the density healing length ξ_n. Also in the FM phase the core of the singly quantized vortex can avoid the density depletion. However, here the defect cannot split. Instead, filling of the vortex core happens by local rotation of the spin vector around the vortex line. The overall structure maintains the axial symmetry of the vortex core.

Interface-crossing singly quantized vortex: when part of the condensate is forced into the FM phase by a linear Zeeman shift, these deformation mechanisms lead to a complex, energetically stable vortex configuration as the energy of an interface-crossing singly quantized vortex relaxes (figure 2, left). The splitting instability leads to the formation of two vortex lines filled with the FM phase on the polar side of the interface. In the FM region, the vortex core fills with the polar phase in order to lower its energy. The filling of the core is made possible by a local rotation of the spin vector close to the vortex line. The resulting spin profile connects smoothly to the spin vector in the FM cores of the polar vortices at the interface.

Half-quantum vortex to singular FM vortex: a similar penetration of the FM phase through the interface to fill the singular line in the polar order parameter occurs in the energetically stable connection of a polar half-quantum vortex to a singular FM vortex (figure 2, middle and right). Simultaneously, the singularity in the FM phase fills with the polar phase in order to minimize its associated gradient energy. Consequently, at the perforation of the interface the two core structures meet and connect to the ground-state phase on the other side of the boundary. Figure 2 also shows that the qualitative features of the defect connection is not contingent on a sharply defined interface region, which is a general feature of our stable defect configurations.

Singly quantized (or half-quantum) vortex to coreless vortex: in the purely FM spin-1 BEC, the singular vortex can be energetically (meta-)stable, but a lower-energy coreless vortex generally exists for the same parameters [50]. One might therefore expect stable states to exist where a coreless vortex connects across the FM-polar interface to a singly quantized (or half-quantum) polar vortex. However, the linear Zeeman shift that is employed here to realize the FM phase when $c_2 > 0$ makes the fountain-like spin texture of the coreless vortex energetically
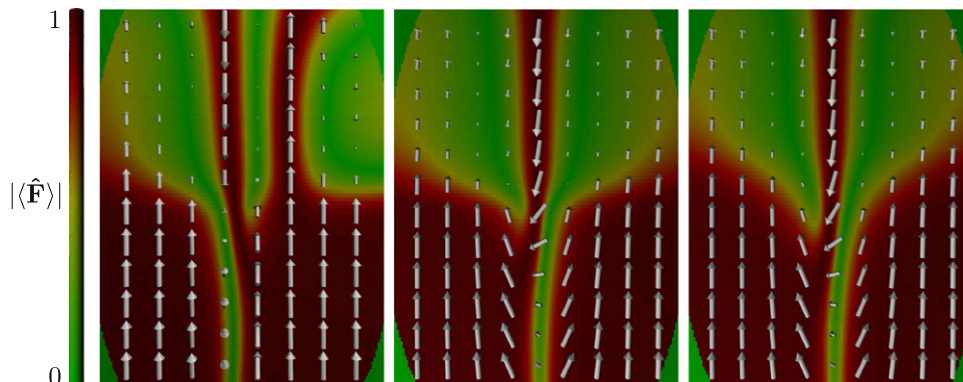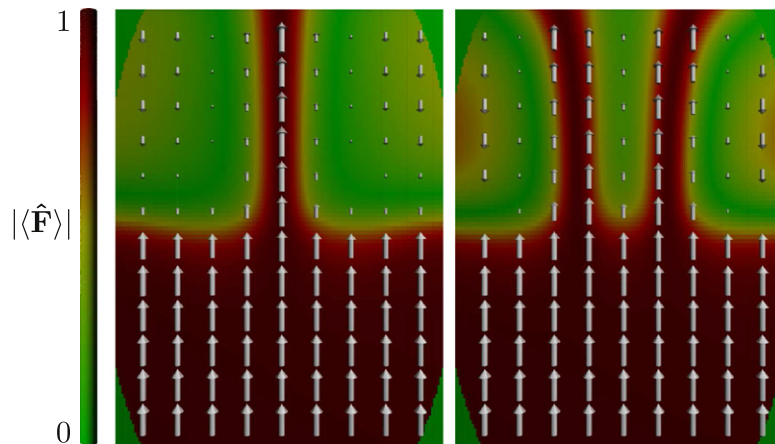
Figure 2. Spin vector (arrows) and spin magnitude (colour gradient) in the energetically stable connection of a singly quantized (left) or half-quantum (middle and right) polar vortex to a singly quantized FM vortex. In the former case the core of the singly quantized polar vortex lowers its energy by splitting into a pair of half-quantum vortices. The singular FM vortex reduces the energy of the core by filling with the polar phase at the singularity. Across the interface region, the linear Zeeman shift varies as $1.0 \times 10^{-3}\hbar\omega \leqslant p \leqslant 0.6\hbar\omega$, with a constant quadratic shift $q = -1.0 \times 10^{-4}\hbar\omega$. The linear shift varies between the polar and FM limits over a distance $1.0l_\perp$ (left and middle) and $4.0l_\perp$ (right), respectively, showing that the qualitative defect structure is insensitive to the width of the interface region. The rotation frequency of the system is $\Omega = 0.22\omega$ for the singly quantized polar vortex and $\Omega = 0.20\omega$ for the half-quantum vortex.

unfavourable. As a consequence, we find all vortex connections involving a coreless vortex on the FM side to be unstable.

Terminating polar vortices: the constructions in section 3 (table 1) demonstrate that it is also possible for polar vortices to terminate at the interface. The terminating half-quantum vortex is energetically stable, and the relaxed core structure is shown in figure 3 (left). In the vortex-free FM region, the linear Zeeman energy causes $\langle \hat{\mathbf{F}} \rangle$ to align with the z axis, and the FM phase penetrates the interface to fill the singular core of the polar vortex. Also a terminating singly quantized vortex results in a stable defect configuration (figure 3, right). In this case, however, relaxation of the energy causes the singly-quantized vortex to split (preserving topology) into a pair of half-quantum vortices, whose singular cores fill with the FM phase.

A singular FM vortex terminating as a point defect exhibits a particularly non-trivial deformation of the defect core as the energy relaxes. In order for the core of the point defect to fill with the FM phase, it deforms into a line defect that forms a ring-shaped vortex (figure 4) attached to the interface [61, 62]. This is a consequence of the 'hairy-ball theorem': if the core of the point defect were to fill with the FM phase, the spin vector in the core would have to be everywhere perpendicular to the radial $\hat{\mathbf{d}}$-vector, which is not possible. After the deformation, a disclination plane in $\hat{\mathbf{d}}$ may be identified, such that on any closed loop through the arch formed by the defect, $\hat{\mathbf{d}}$ winds into $-\hat{\mathbf{d}}$. Hence, the line defect is a half-quantum vortex, and the charge of the point defect is preserved away from the vortex arch. This phenomenon is closely related to the similar deformation of a spherically symmetric point defect into a half-quantum vortex ring—an Alice ring—in the polar spin-1 BEC [40]. The deformation of the point defect into a semi-circular 'Alice arch' on the interface was analyzed also in [61, 62], and our result here

Figure 3. Spin vector (arrows) and spin magnitude (colour gradient) showing an energetically stable half-quantum (left) or singly quantized (right) polar vortex terminating at the interface between the polar and FM parts of the condensate. Energy relaxation causes the singly quantized vortex to split into a pair of half-quantum vortices. The linear shift varies over $1.0 \times 10^{-3}\hbar\omega \leqslant p \leqslant 0.5\hbar\omega$ across an interface of width $1.0l_\perp$, with $q = -1.0 \times 10^{-4}\hbar\omega$. The system rotates at $\Omega = 0.22\omega$ for the singly-quantized polar vortex and $\Omega = 0.2\omega$ for the half-quantum vortex.
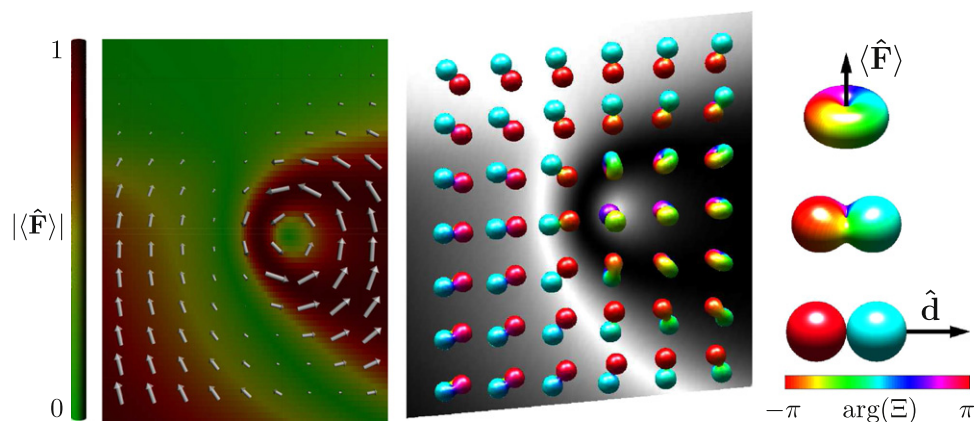
Figure 4. Left: Spin texture (arrows) and magnitude profile (colour gradient) for the polar monopole in a polar BEC with interface created by varying linear Zeeman splitting. Right: the order-parameter symmetry is shown by mapping ζ onto the $Y_{1,m}$ spherical harmonics [83]. The function $\Xi(\theta, \varphi) = \sum_m \zeta_m Y_{1,m}(\theta, \varphi)$ is shown on the far right for the FM (top) and polar (bottom) phases and for intermediate $\left|\left\langle \hat{\mathbf{F}} \right\rangle\right|$, indicating the $\hat{\mathbf{d}}$-vector. In the relaxed defect state, $\hat{\mathbf{d}}$ passes through the arch and points radially away outside it, preserving the monopole charge. Spin magnitude indicated in grey scale. Parameters are $1.0 \times 10^{-3}\hbar\omega \leqslant p \leqslant 0.3\hbar\omega$, for $q = -1.0 \times 10^{-4}\hbar\omega$ in a non-rotating system with interface width $1.0l_\perp$.

demonstrates that it could be engineered by the Zeeman energy shifts. Although the defect is stable in the bulk medium, the density gradient in the trapped condensate causes the arch-shaped line defect to be unstable towards drifting out of the cloud, since a smaller atom density lowers the gradient energy associated with the core. The defect could be stabilized by reversing the density gradient with a pinning laser [40].

Other defect connections described in table 1 are found to be energetically unstable. These include, in addition to FM coreless vortices, also connections involving nematic corelss vortices and Dirac monopoles.

So far we have considered the energy minimization of initially prepared vortex configurations. In a sufficiently rapidly rotating system, vortices may also nucleate. In the polar interaction regime, at low enough rotation frequency, we observe nucleation of a single half-quantum vortex that terminates at the interface. One might expect this to connect across the interface to a coreless vortex in the FM phase. However, this configuration is energetically less favourable, due to the linear Zeeman-energy cost of forming the fountain-like coreless spin texture.

6.2. FM interactions

We now explore the stability properties and core structures in the FM interaction regime ($c_2 < 0$), as for ^{87}Rb. Due to the different ground-state properties of the interpolating solutions, the interface is now created by a non-uniform quadratic Zeeman shift that forces the condensate into the polar phase. Correspondingly we minimize the energy of the defect solutions of section 4 and the corresponding phase-imprinted configurations of section 5.

Coreless vortex to polar singly quantized vortex: contrary to the polar interaction regime, we now do find an energetically stable connection of a coreless vortex on the FM side of the interface to a polar singly quantized vortex (figure 5), as the energy of the initial state (19) relaxes. One might again expect the singly quantized vortex in the polar phase to split into a pair of half-quantum vortices in order to lower the energy of the core. However, the splitting is energetically unfavourable due to the positive quadratic Zeeman shift needed to realize the polar phase in the BEC with FM interactions, which seeks to align $\hat{\mathbf{d}}$ with the z axis, resulting in an effective two-component regime. Accordingly, the stable configuration exhibits an axially symmetric single core with the atoms reaching the FM phase at the line singularity. The spin texture of the coreless vortex connects smoothly to a similar spin texture inside the core of the polar vortex, and is qualitatively independent of the width of the interface region, as shown in figure 5.

Previous studies of singly quantized polar vortices have shown that stable structures in the absence of the interface would favour core structures where the vortex line is split into a pair of half-quantum vortices [50]. Here the existence of both split and unsplit cores, with entirely different symmetries, as stable vortex cores is reminiscent of the vortex core structures of superfluid liquid ^{3}He [73]. In superfluid liquid ^{3}He, the core of a singular B-phase vortex may retain a non-vanishing superfluid density by filling with the A phase. This may appear as an axially symmetric core [74] at high pressure or with a broken axial symmetry [75, 76], as experimentally observed in [99].

Interface-crossing singly quantized vortex: the connection of a singly quantized polar vortex in a uniform $\hat{\mathbf{d}}$ texture to a singular FM vortex is not energetically stable, again in
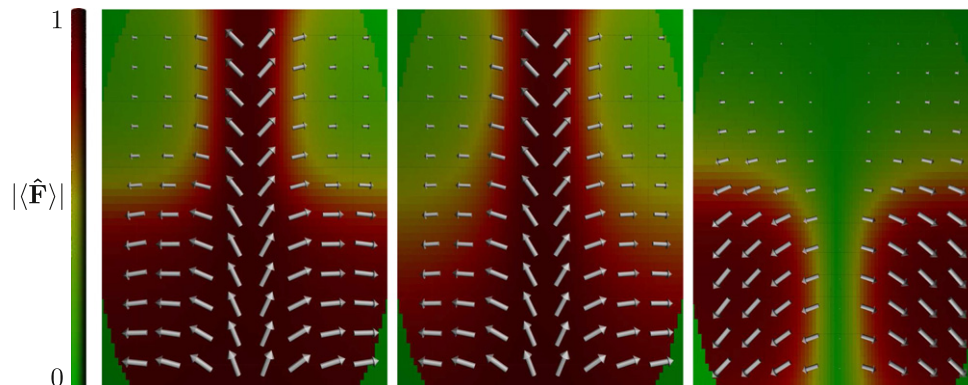
Figure 5. Left and middle: spin texture (arrows) and spin magnitude (colour gradient) of an energetically stable coreless vortex connecting to a singly quantized polar vortex in a system rotating at $\Omega = 0.18\omega$. The width of the interpolating region is $2.0l_\perp$ (left) and $10.0l_\perp$ (middle), over which the quadratic energy shift varies as $p \leqslant q \leqslant 0.198\hbar\omega$, for $p = 9.9 \times 10^{-4}\hbar\omega$. The defect structure is qualitatively insensitive to the width of the interface region. Right: a singular FM vortex that terminates at the interface in the system rotating at $\Omega = 0.16\omega$ (remaining parameters same as in the left panel). Also the connection of a singular FM vortex to a nematic coreless vortex relaxes to the state shown as the quadratic Zeeman energy causes the fountain texture of the nematic axis to be lost in the polar region.

contrast to the case for polar interactions. Energy relaxation of the vortex formed as a 2π winding of the condensate phase everywhere causes the initially uniform spin texture in the FM region to deform locally around the singular vortex line, allowing the condensate to avoid the density depletion [50]. The singular vortex can then leave the cloud, nucleating a coreless vortex in the process. Correspondingly, the singly quantized vortex in the polar part picks up a winding of $\hat{\mathbf{d}}$, and the initial defect state decays to the connection of a coreless vortex to a singly quantized polar vortex, similar to figure 5.

Terminating singular FM vortex: a singular FM vortex may also be written as a winding of α alone (for some β), in which case it can terminate at the interface. The configuration relaxes to an energetically stable vortex state whose spin texture is shown in figure 5 (right). The polar phase then penetrates the interface to fill the core of the FM vortex, allowing the core to expand and lower its energy. By including a winding of β, the initial defect state may also represent a nematic coreless vortex (A.7) on the polar side (see table 2). This is, however, not stable, as the fountain texture in $\hat{\mathbf{d}}$ unwinds due to the quadratic Zeeman shift, resulting again in a terminating FM vortex.

Singular FM vortex terminating as a point defect: the relaxed core structure shown in figure 6 exhibits the deformation of the point defect into an arch-shaped half-quantum vortex attached to the interface. This reaches the FM phase at the line singularity, and connects to the spin texture of the FM vortex. The deformation mechanism is here analogous to that discussed in the polar case. Again, the arch-shaped half-quantum vortex maintains its structure, but is unstable towards drifting out of the cloud.

Also in the FM interaction regime, we find that solutions involving a Dirac monopole are energetically unstable. We further find that neither the terminating singly quantized polar vortex
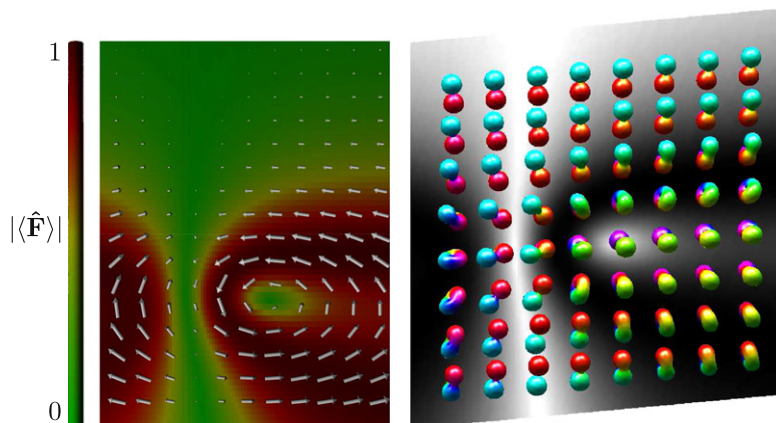
Figure 6. Left: spin texture $\langle \hat{\mathbf{F}} \rangle$ (arrows) and magnitude $\left| \langle \hat{\mathbf{F}} \rangle \right|$ (colour gradient) of a singular FM vortex connecting to a nematic monopole where the interface is induced by quadratic Zeeman splitting. The monopole deforms into a line defect as the energy relaxes. Right: mapping of ζ onto the $Y_{1,m}$ spherical harmonics (see also figure 4), indicating the nematic axis $\hat{\mathbf{d}}$ preserving the charge of the monopole. (Away from the interface region, $\hat{\mathbf{d}}$ tends towards $\pm\hat{\mathbf{z}}$ due to the quadratic Zeeman energy.) Spin magnitude indicated in grey scale. Parameters are $p \leqslant q \leqslant 0.198\hbar\omega$, for $p = 9.9 \times 10^{-4}\hbar\omega$ in a non-rotating system with interface width $2.0l_\perp$.

nor the connection of a coreless vortex to a nematic coreless vortex (see table 2) are energetically stable.

In addition to minimizing the energy of each defect state constructed in section 4, we also performed simulations starting from the corresponding experimentally phase-imprintable defect states constructed from vortex lines and soliton planes in section 5. In each case, the relaxed defect state agrees with those resulting from the defect wave functions of section 4.

As in the polar interaction case, we may also start from a vortex-free configuration and study nucleation of defects as a result of rotation. For weak rotation we here find nucleation of a singly quantized polar vortex that connects to a coreless vortex in the FM region. The stable polar vortex core again preserves the axial symmetry.

7. Concluding remarks

In conclusion, we propose that a stable, coherent interface between topologically dissimilar regions of atomic spinor systems can be engineered by spatially non-uniform linear or quadratic Zeeman shifts, which are commonly manipulated in experiments. As a particular example we have shown how an interface can be established between FM and polar regions of a spin-1 BEC. We have derived analytic expressions for states representing continuous defect connections across the interface, interpolating between FM and polar topology in terms of either the linear (for $c_2 > 0$) or quadratic (for $c_2 < 0$) Zeeman shifts. We have demonstrated the energetic stability of several non-trivial interface-crossing defect states.

In the present simulations we did not conserve the longitudinal condensate magnetization. In physical systems where *s*-wave scattering is the dominant relaxation mechanism (compared

with, e.g., dipole–dipole interactions or collisions with high-temperature atoms), the magnetization is preserved on experimentally relevant time scales [68, 100]. Our recent study of coreless vortices [51], however, indicates that the conservation of magnetization only plays an important role in situations where the initial value of the magnetization differs substantially from the final magnetization values obtained in simulations with unconstrained magnetization. For typical vortex states such conditions can easily be avoided.

There are several obvious possibilities for extending our study. The atomic spins generate magnetic dipole moments. Depending on the atom, these give rise to dipole–dipole interactions in the condensate, which may influence the structure of textures and defects [48, 55]. Simulations incorporating these dipole–dipole interactions can be performed by introducing non-local interactions in the numerical model. On the other hand, defect formation in annihilation of colliding interfaces could mimic brane annihilation scenarios [6, 7]. Furthermore, defects and textures can be considerably more complex in spin-2 and spin-3 systems that, for instance, have non-Abelian vortices [53, 54]. This is likely to result also in richer interface physics. In strongly correlated scenarios, the atoms may also be confined in optical lattices in such a way that interfaces could separate different lattice regions, each simultaneously exhibiting a different phase of quantum magnetism.

Acknowledgments

Appendix A. Elementary vortex solutions

In this appendix we provide for reference a brief overview of the elementary defect states of the spin-1 BEC in the pure FM and polar phases. For a more detailed presentation, see, e.g., [62, 83].

In the FM phase, all degenerate, physically distinguishable spinors are related by three-dimensional spin rotations given by Euler angles α, β and γ, where the third Euler angle is absorbed by the condensate phase in $\phi' = \phi - \gamma$. Consequently, an arbitrary FM spinor can be constructed by applying a spin rotation to a reference spinor $\zeta = \left(1, 0, 0\right)^T$ to arrive at (3), with spin vector $\left\langle \hat{\mathbf{F}} \right\rangle = \cos\alpha \sin\beta \hat{\mathbf{x}} + \sin\alpha \sin\beta \hat{\mathbf{y}} + \cos\beta \hat{\mathbf{z}}$. From this general expression, we can construct the non-trivial representatives of the two classes of line defects supported by the corresponding $\mathrm{SO}\left(3\right)$ ground-state manifold.

The simplest singular vortex corresponds to a 2π winding of the condensate phase ϕ' in a uniform spin texture. This phase vortex is simply described by letting $\phi' = \varphi$, the azimuthal angle, in (3), keeping α and β constant. However, other, topologically equivalent, singular vortices can be constructed from the phase vortex by local spin rotations. We may, for example, rotate the spins into a disgyration corresponding to $\alpha = \varphi$:

$$\zeta^{\mathrm{sv}} = \frac{1}{\sqrt{2}} \begin{pmatrix} \sqrt{2}\, e^{-i\varphi} \cos^2\frac{\beta}{2} \\ \sin\beta \\ \sqrt{2}\, e^{i\varphi} \sin^2\frac{\beta}{2} \end{pmatrix}. \tag{A.1}$$

When $\beta = 0$ the spins align with the z axis, and the singular spin texture coincides with a phase vortex. However, for $\beta \neq 0$ the spins tilt radially away from the z axis, and at $\beta = \pi/2$ form a radial spin disgyration (spin vortex) that is singular, but carries no mass circulation.

The fact that mass circulation alone is not quantized in the FM phase makes it possible for angular momentum to be carried by non-singular coreless vortices. The prototypical coreless vortex is characterized by a fountain-like spin texture, where the spin aligns with the z axis on the vortex line, and tilts radially away from it with increasing radial distance ρ, corresponding to a monotonically increasing $\beta(\rho)$. The wave function is kept non-singular everywhere by a combined rotation of the spin and the condensate phase, $\alpha = \phi' = \varphi$, to form

$$\zeta^{\mathrm{cl}}(\mathbf{r}) = \frac{1}{\sqrt{2}} \begin{pmatrix} \sqrt{2}\, \cos^2\frac{\beta(\rho)}{2} \\ e^{i\varphi} \sin\beta(\rho) \\ \sqrt{2}\, e^{2i\varphi} \sin^2\frac{\beta(\rho)}{2} \end{pmatrix}. \tag{A.2}$$

Similarly to the singular vortices, several non-singular vortices are possible. These are all related to (A.2), and to the vortex-free state, by local spin rotations.

It is further possible to rotate the spins in the coreless vortex to point everywhere radially away from the origin, resulting in a terminating, doubly quantized vortex line. This hedgehog configuration, $\langle \hat{\mathbf{F}} \rangle = \hat{\mathbf{r}}$, is analogous [41, 42, 47] to the Dirac magnetic monopole [101], with the doubly quantized vortex line corresponding to the attached Dirac string. When the Dirac string coincides with the positive z axis, the corresponding spinor is

$$\zeta^{\mathrm{D}} = \frac{1}{\sqrt{2}} \begin{pmatrix} \sqrt{2}\, e^{-2i\varphi} \cos^2\frac{\theta}{2} \\ e^{-i\varphi} \sin\theta \\ \sqrt{2}\, \sin^2\frac{\theta}{2} \end{pmatrix}, \tag{A.3}$$

where we have set $\alpha = \varphi$ and $\beta = \theta$, the polar angle, to form the hedgehog texture, and chosen $\phi' = -\varphi$. The Dirac string may instead be aligned with the negative z axis by instead choosing $\phi' = \varphi$.

In the polar phase, the order parameter is determined by the condensate phase and rotations of the nematic axis $\hat{\mathbf{d}}$, which may be applied to the reference state $\zeta = (0, 1, 0)^T$, with $\hat{\mathbf{d}} = \hat{\mathbf{z}}$, to yield

$$\zeta^{\mathrm{p}} = \frac{e^{i\phi}}{\sqrt{2}} \begin{pmatrix} -e^{-i\alpha} \sin\beta \\ \sqrt{2}\, \cos\beta \\ e^{i\alpha} \sin\beta \end{pmatrix}, \tag{A.4}$$

whose equivalence to (4) follows from the identification $\hat{\mathbf{d}} = \cos\alpha \sin\beta\, \hat{\mathbf{x}} + \sin\alpha \sin\beta\, \hat{\mathbf{y}} + \cos\beta\, \hat{\mathbf{z}}$. Note that the choice of reference state corresponds to the polar limit of (7), and

the Euler angles in (A.4) therefore acquire the same meaning as in the polar limit of (15). [In the polar limit of (10), the spin rotation is instead applied to the spinor $\zeta = \left(-1/\sqrt{2},\, 0,\, 1/\sqrt{2} \right)^T$ with $\hat{\mathbf{d}} = \hat{\mathbf{x}}$, and the relation between $\hat{\mathbf{d}}$ and the Euler angles is modified accordingly.]

In the polar phase, all circulation-carrying vortices are singular. The simplest is again a singly quantized vortex in a uniform $\hat{\mathbf{d}}$-texture, constructed as $\phi = \varphi$ in (A.4). However, rotations of $\hat{\mathbf{d}}$ do not contribute to the quantized circulation, and hence a singly quantized vortex may be accompanied by a winding of $\hat{\mathbf{d}}$ as long as ζ remains single valued. For example, the choice $\phi = \alpha = \varphi$ results in

$$\zeta^{1'} = \frac{1}{\sqrt{2}} \begin{pmatrix} -\sin\beta \\ \sqrt{2}\, e^{i\varphi} \cos\beta \\ e^{2i\varphi} \sin\beta \end{pmatrix}, \tag{A.5}$$

which a singly quantized vortex with a 2π winding in $\hat{\mathbf{d}}$.

Due to the nematic order $\zeta\left(\phi, \hat{\mathbf{d}}\right) = \zeta\left(\phi + \pi, -\hat{\mathbf{d}}\right)$, the single quantum is not the smallest unit of circulation in the polar phase. By combining a π winding of the condensate phase with a $\hat{\mathbf{d}} \to -\hat{\mathbf{d}}$ winding of the nematic axis, one can construct a vortex carrying half a quantum of circulation. The simplest such vortex, where $\hat{\mathbf{d}}$ is confined to the xy plane, is represented by

$$\zeta^{\mathrm{hq}} = \frac{e^{i\varphi/2}}{\sqrt{2}} \begin{pmatrix} -e^{-i\varphi/2} \\ 0 \\ e^{i\varphi/2} \end{pmatrix} = \frac{1}{\sqrt{2}} \begin{pmatrix} -1 \\ 0 \\ e^{i\varphi} \end{pmatrix}. \tag{A.6}$$

In general, a half-quantum vortex may exhibit a more complicated $\hat{\mathbf{d}}$-field, provided that $\hat{\mathbf{d}} \to -\hat{\mathbf{d}}$ on any closed loop around the vortex line.

Even though circulation is quantized in the polar phase, it is possible to form a non-singular nematic coreless vortex [51] that does not carry angular momentum. Here $\hat{\mathbf{d}}$ forms a fountain-like texture analogous to the FM coreless vortex. This structure was recently experimentally phase imprinted [22, 23]. From (A.4) it can be constructed by choosing $\alpha = \varphi$ combined with $\beta(\rho)$ increasing monotonically from $\beta(0) = 0$ to form

$$\zeta^{\mathrm{p}} = \frac{1}{\sqrt{2}} \begin{pmatrix} -e^{-i\varphi} \sin\beta(\rho) \\ \sqrt{2} \cos\beta(\rho) \\ e^{i\varphi} \sin\beta(\rho) \end{pmatrix}. \tag{A.7}$$

The polar phase also supports singular point defects (monopoles). The basic monopole solution is the spherically symmetric $\hat{\mathbf{d}} = \hat{\mathbf{r}}$ texture, which is analogous to the 't Hooft–Polyakov monopole in quantum field theory. It is represented by the spinor

$$\zeta^{\mathrm{pm}} = \frac{1}{\sqrt{2}} \begin{pmatrix} - e^{-i\varphi} \sin \theta \\ \sqrt{2} \cos \theta \\ e^{i\varphi} \sin \theta \end{pmatrix}. \tag{A.8}$$

References

[1] Salomaa M M 1987 Monopoles in the rotating superfluid helium-3 AB interface *Nature* **326** 367–70

[2] Volovik G E 2003 *The Universe in a Helium Droplet* (Oxford: Oxford University Press)

[3] Finne A P, Eltsov V B, Hänninen R, Kopnin N B, Kopu J, Krusius M, Tsubota M and Volovik G E 2006 Dynamics of vortices and interfaces in superfluid ^{3}He *Rep. Prog. Phys.* **69** 3157–230

[4] Kibble T W B 1976 Topology of cosmic domains and strings *J. Phys. A: Math. Gen.* **9** 1387–98

[5] Vilenkin A and Shellard E P S 1994 *Cosmic Strings and Other Topological Defects* (Cambridge: Cambridge University Press)

[6] Dvali G and Tye S-H H 1999 Brane inflation *Phys. Lett.* B **450** 72–82

[7] Sarangi S and Tye S-H H 2002 Cosmic string production towards the end of brane inflation *Phys. Lett.* B **536** 185–92

[8] Bert J A, Kalisky B, Bell C, Kim M, Hikita Y, Hwang H Y and Moler K A 2011 Direct imaging of the coexistence of ferromagnetism and superconductivity at the LaAlO$_3$/SrTiO$_3$ interface *Nat. Phys.* **7** 767–71

[9] Zurek W H 1985 Cosmological experiments in superfluid helium? *Nature* **317** 505–8

[10] Bäuerle C, Bunkov Y M, Fisher S N, Godfrin H and Pickett G R 1996 Laboratory simulation of cosmic string formation in the early universe using superfluid ^{3}He *Nature* **382** 332–4

[11] Ruutu V M H, Eltsov V B, Gill A J, Kibble T W B, Krusius M, Makhlin Y G, Plaais B, Volovik G E and Xu W 1996 Vortex formation in neutron-irradiated superfluid ^{3}He as an analogue of cosmological defect formation *Nature* **382** 334–6

[12] Weiler C N, Neely T W, Scherer D R, Bradley A S, Davis M J and Anderson B P 2008 Spontaneous vortices in the formation of Bose–Einstein condensates *Nature* **455** 948–51

[13] Sadler L E, Higbie J M, Leslie S R, Vengalattore M and Stamper-Kurn D M 2006 Spontaneous symmetry breaking in a quenched ferromagnetic spinor Bose–Einstein condensate *Nature* **443** 312–5

[14] Radu E and Volkov M S 2008 Stationary ring solitons in field theory—knots and vortons *Phys. Rep.* **468** 101–51

[15] Ruostekoski J and Anglin J R 2001 Creating vortex rings and three-dimensional skyrmions in Bose–Einstein condensates *Phys. Rev. Lett.* **86** 3934–7

[16] Battye R A, Cooper N R and Sutcliffe P M 2002 Stable skyrmions in two-component Bose–Einstein condensates *Phys. Rev. Lett.* **88** 080401

[17] Savage C M and Ruostekoski J 2003 Energetically stable particlelike skyrmions in a trapped Bose–Einstein condensate *Phys. Rev. Lett.* **91** 010403

[18] Ruostekoski J 2004 Stable particlelike solitons with multiply quantized vortex lines in Bose–Einstein condensates *Phys. Rev.* A **70** 041601

[19] Kawakami T, Mizushima T, Nitta M and Machida K 2012 Stable skyrmions in SU(2) gauged Bose–Einstein condensates *Phys. Rev. Lett.* **109** 015301

[20] Leanhardt A E, Shin Y, Kielpinski D, Pritchard D E and Ketterle W 2003 Coreless vortex formation in a spinor Bose–Einstein condensate *Phys. Rev. Lett.* **90** 140403

[21] Leslie L S, Hansen A, Wright K C, Deutsch B M and Bigelow N P 2009 Creation and detection of skyrmions in a Bose–Einstein condensate *Phys. Rev. Lett.* **103** 250401

[22] Choi J-y, Kwon W J and Shin Y-I 2012 Observation of topologically stable 2D skyrmions in an antiferromagnetic spinor Bose–Einstein condensate *Phys. Rev. Lett.* **108** 035301

[23] Choi J-y, Kwon W J, Lee M, Jeong H, An K and Shin Y-i 2012 Imprinting skyrmion spin textures in spinor Bose–Einstein condensates *New J. Phys.* **14** 053013

[24] Vengalattore M, Leslie S R, Guzman J and Stamper-Kurn D M 2008 Spontaneously modulated spin textures in a dipolar spinor Bose–Einstein condensate *Phys. Rev. Lett.* **100** 170403

[25] Kronjäger J, Becker C, Soltan-Panahi P, Bongs K and Sengstock K 2010 Spontaneous pattern formation in an antiferromagnetic quantum gas *Phys. Rev. Lett.* **105** 090402

[26] Bookjans E M, Vinit A and Raman C 2011 Quantum phase transition in an antiferromagnetic spinor Bose–Einstein condensate *Phys. Rev. Lett.* **107** 195306

[27] Guzman J, Jo G-B, Wenz A N, Murch K W, Thomas C K and Stamper-Kurn D M 2011 Long-time-scale dynamics of spin textures in a degenerate $F = 1$ ^{87}Rb spinor bose gas *Phys. Rev. A* **84** 063625

[28] Khawaja U A and Stoof H 2001 Skyrmions in a ferromagnetic Bose–Einstein condensate *Nature* **411** 918–20

[29] Mueller E J and Ho T-L 2002 Two-component Bose–Einstein condensates with a large number of vortices *Phys. Rev. Lett.* **88** 180403

[30] Kasamatsu K, Tsubota M and Ueda M 2003 Vortex phase diagram in rotating two-component Bose–Einstein condensates *Phys. Rev. Lett.* **91** 150406

[31] Mason P and Aftalion A 2011 Classification of the ground states and topological defects in a rotating two-component Bose–Einstein condensate *Phys. Rev. A* **84** 033611

[32] Ho T-L 1998 Spinor Bose condensates in optical traps *Phys. Rev. Lett.* **81** 742

[33] Ohmi T and Machida K 1998 Bose–Einstein condensation with internal degrees of freedom in alkali atom gases *J. Phys. Soc. Jpn* **67** 1822–5

[34] Yip S-K 1999 Internal vortex structure of a trapped spinor Bose–Einstein condensate *Phys. Rev. Lett.* **83** 4677

[35] Leonhardt U and Volovik G 2000 *JETP Lett.* **72** 46–48

[36] Mizushima T, Machida K and Kita T 2002 Mermin-Ho vortex in ferromagnetic spinor Bose–Einstein condensates *Phys. Rev. Lett.* **89** 030401

[37] Martikainen J-P, Collin A and Suominen K-A 2002 Coreless vortex ground state of the rotating spinor condensate *Phys. Rev. A* **66** 053604

[38] Zhou F 2003 Quantum spin nematic states in Bose–Einstein condensates *Int. J. Mod. Phys.* B **17** 2643–98

[39] Stoof H T C, Vliegen E and Al Khawaja U 2001 Monopoles in an antiferromagnetic Bose–Einstein condensate *Phys. Rev. Lett.* **87** 120407

[40] Ruostekoski J and Anglin J R 2003 Monopole core instability and alice rings in spinor Bose–Einstein condensates *Phys. Rev. Lett.* **91** 190402

[41] Savage C M and Ruostekoski J 2003 Dirac monopoles and dipoles in ferromagnetic spinor Bose–Einstein condensates *Phys. Rev. A* **68** 043604

[42] Pietilä V and Möttönen M 2009 Creation of Dirac monopoles in spinor Bose–Einstein condensates *Phys. Rev. Lett.* **103** 030401

[43] Reijnders J W, van Lankvelt F J M, Schoutens K and Read N 2004 Rotating spin-1 bosons in the lowest Landau level *Phys. Rev. A* **69** 023612

[44] Mueller E J 2004 Spin textures in slowly rotating Bose–Einstein condensates *Phys. Rev. A* **69** 033606

[45] Saito H, Kawaguchi Y and Ueda M 2006 Breaking of chiral symmetry and spontaneous rotation in a spinor Bose–Einstein condensate *Phys. Rev. Lett.* **96** 065302

[46] Takahashi M, Pietilä V, Möttönen M, Mizushima T and Machida K 2009 Vortex-splitting and phase-separating instabilities of coreless vortices in $F = 1$ spinor Bose–Einstein condensates *Phys. Rev. A* **79** 023618

[47] Ruokokoski E, Pietilä V and Möttönen M 2011 Ground-state Dirac monopole *Phys. Rev. A* **84** 063627

[48] Simula T P, Huhtamäki J A M, Takahashi M, Mizushima T and Machida K 2011 Rotating dipolar spin-1 Bose–Einstein condensates *J. Phys. Soc. Jpn* **80** 013001

[49] Kobayashi S, Kawaguchi Y, Nitta M and Ueda M 2012 Topological classification of vortex-core structures of spin-1 Bose–Einstein condensates *Phys. Rev.* A **86** 023612

[50] Lovegrove J, Borgh M O and Ruostekoski J 2012 Energetically stable singular vortex cores in an atomic spin-1 Bose–Einstein condensate *Phys. Rev.* A **86** 013613

[51] Lovegrove J, Borgh M O and Ruostekoski J 2014 Energetic stability of coreless vortices in spin-1 Bose–Einstein condensates with conserved magnetization *Phys. Rev. Lett.* **112** 075301

[52] Semenoff G W and Zhou F 2007 Discrete symmetries and 1/3-quantum vortices in condensates of $F = 2$ cold atoms *Phys. Rev. Lett.* **98** 100401

[53] Huhtamäki J A M, Simula T P, Kobayashi M and Machida K 2009 Stable fractional vortices in the cyclic states of Bose–Einstein condensates *Phys. Rev.* A **80** 051601

[54] Kobayashi M, Kawaguchi Y, Nitta M and Ueda M 2009 Collision dynamics and rung formation of non-Abelian vortices *Phys. Rev. Lett.* **103** 115301

[55] Santos L and Pfau T 2006 Spin-3 chromium Bose–Einstein condensates *Phys. Rev. Lett.* **96** 190404

[56] Barnett R, Turner A and Demler E 2007 Classifying vortices in $S = 3$ Bose–Einstein condensates *Phys. Rev.* A **76** 013605

[57] Bogomolny E B 1976 Stability of classical solutions *Sov. J. Nucl. Phys.* **24** 449

[58] Jackiw R and Rebbi C 1976 Solitons with fermion number 1/2 *Phys. Rev.* D **13** 3398–409

[59] Manton N and Sutcliffe P 2004 *Topological Solitons* (Cambridge: Cambridge University Press)

[60] Faddeev L and Niemi A J 1997 Stable knot-like structures in classical field theory *Nature* **387** 58–61

[61] Borgh M O and Ruostekoski J 2012 Topological interface engineering and defect crossing in ultracold atomic gases *Phys. Rev. Lett.* **109** 015302

[62] Borgh M O and Ruostekoski J 2013 Topological interface physics of defects and textures in spinor Bose–Einstein condensates *Phys. Rev.* A **87** 033617

[63] Kasamatsu K, Takeuchi H, Nitta M and Tsubota M 2010 Analogues of D-branes in Bose–Einstein condensates *J. High Energy Phys.* **011** 068

[64] Takeuch H, Kasamatsu K, Nitta M and Tsubota M 2011 Vortex formations from domain wall annihilations in two-component Bose–Einstein condensates *J. Low Temp. Phys.* **162** 243–9

[65] Nitta M, Kasamatsu K, Tsubota M and Takeuchi H 2012 Creating vortons and three-dimensional skyrmions from domain-wall annihilation with stretched vortices in Bose–Einstein condensates *Phys. Rev.* A **85** 053639

[66] Takeuchi H, Kasamatsu K, Tsubota M and Nitta M 2012 Tachyon condensation due to domain-wall annihilation in Bose–Einstein condensates *Phys. Rev. Lett.* **109** 245301

[67] Kasamatsu K, Takeuchi H and Nitta M 2013 D-brane solitons and boojums in field theory and Bose–Einstein condensates *J. Phys.: Condens. Matter* **25** 404213

[68] Stenger J, Inouye S, Stamper-Kurn D M, Miesner H-J, Chikkatur A P and Ketterle W 1998 Spin domains in ground-state Bose–Einstein condensates *Nature* **396** 345–8

[69] Koashi M and Ueda M 2000 Exact eigenstates and magnetic response of spin-1 and spin-2 Bose–Einstein condensates *Phys. Rev. Lett.* **84** 1066

[70] Zhang W, Yi S and You L 2003 Mean field ground state of a spin-1 condensate in a magnetic field *New J. Phys.* **5** 77

[71] Murata K, Saito H and Ueda M 2007 Broken-axisymmetry phase of a spin-1 ferromagnetic Bose–Einstein condensate *Phys. Rev.* A **75** 013607

[72] Ruostekoski J and Dutton Z 2007 Dynamical and energetic instabilities in multicomponent Bose–Einstein condensates in optical lattices *Phys. Rev.* A **76** 063607

[73] Salomaa M M and Volovik G E 1987 Quantized vortices in superfluid ^{3}He *Rev. Mod. Phys.* **59** 533–613

[74] Salomaa M M and Volovik G E 1983 Vortices with ferromagnetic superfluid core in ^{3}He-*B Phys. Rev. Lett.* **51** 2040–3

[75] Salomaa M M and Volovik G E 1986 Vortices with spontaneously broken axisymmetry in ³He-*B Phys. Rev. Lett.* **56** 363–6

[76] Thuneberg E V 1986 Identification of vortices in superfluid ³He-*B Phys. Rev. Lett.* **56** 359–62

[77] 't Hooft G 1974 Magnetic monopoles in unified gauge theories *Nucl. Phys.* B **79** 276–84

[78] Polyakov A 1974 Particle spectrum in quantum field theory *JETP Lett.* **20** 194

[79] Vollhardt D and Wölfle P 1990 *The Superfluid Phases of Helium 3* (London: Taylor and Francis)

[80] Mermin N D 1977 Surface singularities and superflow in ³He-A *Quantum Fluids and Solids* ed S B Trickey, E D Adams and J W Dufty (New York: Plenum) pp 3–22

[81] Gerbier F, Widera A, Fölling S, Mandel O and Bloch I 2006 Resonant control of spin dynamics in ultracold quantum gases by microwave dressing *Phys. Rev.* A **73** 041602

[82] Bradley D I, Fisher S N, Guenault A M, Haley R P, Kopu J, Martin H, Pickett G R, Roberts J E and Tsepelin V 2008 Relic topological defects from brane annihilation simulated in superfluid ³He *Nat. Phys.* **4** 46–9

[83] Kawaguchi Y and Ueda M 2012 Spinor Bose–Einstein condensates *Phys. Rep.* **520** 253–381

[84] Corney A 1977 *Atomic and Laser Spectroscopy* (Oxford: Oxford University Press)

[85] Santos L, Fattori M, Stuhler J and Pfau T 2007 Spinor condensates with a laser-induced quadratic Zeeman effect *Phys. Rev.* A **75** 053606

[86] Bolda E L and Walls D F 1998 Creation of vortices in a Bose–Einstein condensate by a Raman technique *Phys. Lett.* A **246** 32–6

[87] Marzlin K-P, Zhang W and Wright E M 1997 Vortex coupler for atomic Bose–Einstein condensates *Phys. Rev. Lett.* **79** 4728–31

[88] Dutton Z and Ruostekoski J 2004 Transfer and storage of vortex states in light and matter waves *Phys. Rev. Lett.* **93** 193602

[89] Williams J E and Holland M J 1999 Preparing topological states of a Bose–Einstein condensate *Nature* **401** 568–72

[90] Isoshima T, Nakahara M, Ohmi T and Machida K 2000 Creation of a persistent current and vortex in a Bose–Einstein condensate of alkali-metal atoms *Phys. Rev.* A **61** 063610

[91] Matthews M R, Anderson B P, Haljan P C, Hall D S, Wieman C E and Cornell E A 1999 Vortices in a Bose–Einstein condensate *Phys. Rev. Lett.* **83** 2498–501

[92] Leanhardt A E, Görlitz A, Chikkatur A P, Kielpinski D, Shin Y, Pritchard D E and Ketterle W 2002 Imprinting vortices in a Bose–Einstein condensate using topological phases *Phys. Rev. Lett.* **89** 190403

[93] Shin Y, Saba M, Vengalattore M, Pasquini T A, Sanner C, Leanhardt A E, Prentiss M, Pritchard D E and Ketterle W 2004 Dynamical instability of a doubly quantized vortex in a Bose–Einstein condensate *Phys. Rev. Lett.* **93** 160406

[94] Andersen M F, Ryu C, Cladé P, Natarajan V, Vaziri A, Helmerson K and Phillips W D 2006 Quantized rotation of atoms from photons with orbital angular momentum *Phys. Rev. Lett.* **97** 170406

[95] Burger S, Bongs K, Dettmer S, Ertmer W, Sengstock K, Sanpera A, Shlyapnikov G V and Lewenstein M 1999 Dark solitons in Bose–Einstein condensates *Phys. Rev. Lett.* **83** 5198–201

[96] Denschlag J *et al* 2000 Generating solitons by phase engineering of a Bose–Einstein condensate *Science* **287** 97–101

[97] Knoop S, Schuster T, Scelle R, Trautmann A, Appmeier J, Oberthaler M K, Tiesinga E and Tiemann E 2011 Feshbach spectroscopy and analysis of the interaction potentials of ultracold sodium *Phys. Rev.* A **83** 042704

[98] van Kempen E G M, Kokkelmans S J J M F, Heinzen D J and Verhaar B J 2002 Interisotope determination of ultracold rubidium interactions from three high-precision experiments *Phys. Rev. Lett.* **88** 093201

[99] Kondo Y, Korhonen J S, Krusius M, Dmitriev V V, Mukharsky Y M, Sonin E B and Volovik G E 1991 Direct observation of the nonaxisymmetric vortex in superfluid ³He-*B Phys. Rev. Lett.* **67** 81–4

[100] Jacob D, Shao L, Corre V, Zibold T, De Sarlo L, Mimoun E, Dalibard J and Gerbier F 2012 Phase diagram of spin-1 antiferromagnetic Bose–Einstein condensates *Phys. Rev.* A **86** 061601

[101] Dirac P A M 1948 The theory of magnetic poles *Phys. Rev.* **74** 817–30